Translational Inelasticity of NO and CO in Scattering from Ultra-Thin Metallic Films of Ag/Au(111)

Christoph Steinsiek[*1], Pranav R. Shirhatti[1,2,3], Jan Geweke[1,2,4], Jascha A. Lau[1,2], Jan Altschäffel[1,2], Alexander Kandratsenka[1,2], Christof Bartels [1,6], Alec M. Wodtke[1,2,4,5].*

[1]Institute for Physical Chemistry, Georg-August University of Göttingen, Tammannstraße 6, 37077 Göttingen, Germany.

[2]Department of Dynamics at Surfaces, Max Planck Institute for Biophysical Chemistry, Am Faßberg 11, 37077 Göttingen, Germany.

[3]Tata Institute of Fundamental Research, 36/P, Gopanapally Village, Serilingampally Mandal, Ranga Reddy District, Hyderabad 500107, India

[4]Max-Planck-EPFL Center for Molecular Nanoscience and Technology, Institute of Chemical Science and Engineering (ISIC), Station 6, ÉcolePolytechniqueFédérale de Lausanne (EPFL), CH-1015 Lausanne, Switzerland.

[5]International Center for Advanced Studies of Energy Conversion, Georg-August University of Göttingen, Tammannstraße 6, 37077 Göttingen, Germany,

[6]Physikalisches Institut, Universität Freiburg, Hermann-Herder-Straße 3, 79104 Freiburg, Germany

Supporting Information

1. Elastic scattering of NO and CO from ultrathin metallic films

NO and CO show very similar behavior in scattering from thin metallic films. For the sake of clarity, only representative data have been presented in the main manuscript. A more complete set of data is provided below.

After fitting the arrival time distributions of NO($v = 2 \rightarrow 2$) scattering as described in the experimental section, we obtained thickness-dependent kinetic energy distributions. Fig. S1 shows such data for clean Au(111) (top panel), the transition between 0-3 ML Ag/Au (central panel) and thicker films > 3 ML (bottom panel).

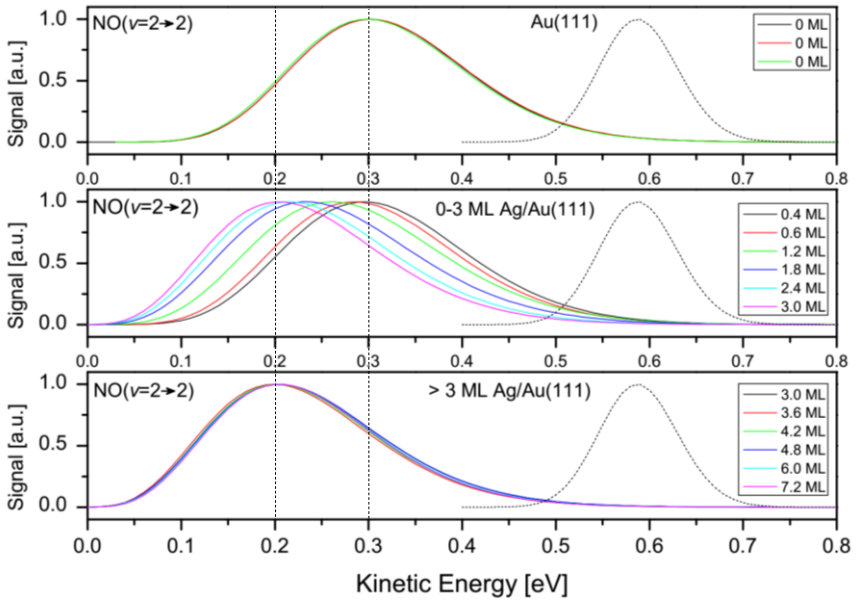

Fig. S1: Kinetic energy distributions of NO($v = 2 \rightarrow 2$) derived from the fits on the data depicted in Figure 3. The transition from Au to Ag exhibits an energy shift of the distribution by ~0.1 eV. The dashed curve describes the kinetic energy distribution of the incident beam.

NO($v = 0 \rightarrow 0$) TOF distributions and fits are displayed in Fig. S2. Those fits were converted into energy space and are plotted in Fig. S3.

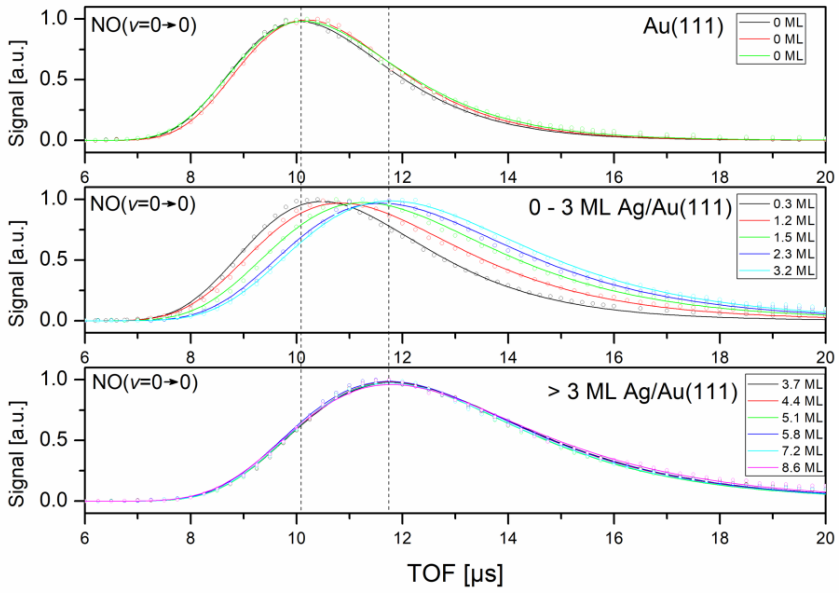

Fig. S2: Arrival time distributions of NO($v = 0 \rightarrow 0$, $J = 6.5$) scattering from 0- 8.6 ML wedge Ag/Au(111). Peak timings of both limiting cases (clean Au and bulk limit of Ag/Au) are marked by two dashed vertical lines.

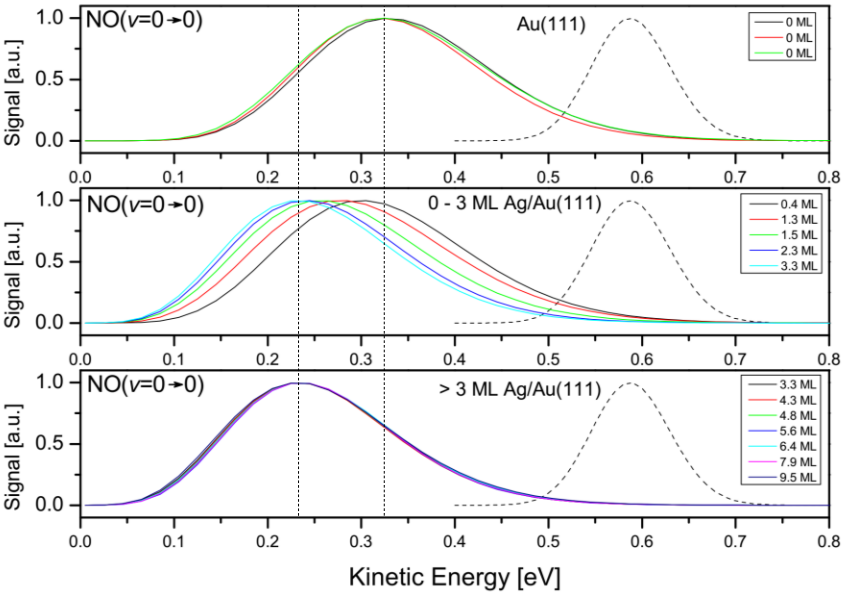

Fig. S3: Kinetic Energy Distributions of NO ($v = 0 \rightarrow 0$, $J = 6.5$) scattering from 0 - 8.6 ML Wedge Ag/Au(111). The distribution of the incoming beam is depicted by a dashed line.

Overall, no distinct difference is observed between elastic scattering of NO($v = 2 \rightarrow 2$) and NO($v = 0 \rightarrow 0$). For both cases (Fig. 3 and Fig. Fig. S2, respectively), the TOF distributions exhibit a broadening and a shift to later times. The kinetic energy distributions (Fig. S2 and Fig. S3, respectively) have approximately the same FWHM and only the shift of the peak is observed. A direct comparison of the thickness-dependent FWHM for both data sets is shown in Fig. S4.

Here, for scattering from pure Au(111) and Ag/Au(111) films above 3 ML thickness, the same FWHM is observed, a feature that we also observed when comparing NO($v = 0 \rightarrow 0$) scattering from bulk Au(111) and bulk Ag(111). One the one hand, this is evidence for a controlled layer-by-layer growth without the formation of three-dimensional structures resulting in increased surface roughness and strong broadening of the kinetic energy distributions. In addition, a weak maximum is observed in the transition region near 1-2 ML. This could indicate that the TOF distributions in this range are actually a mix of molecules scattered from different areas of completed monolayers. As an example, the resulting TOF distribution after scattering from nominal 1.5 ML would consist of one part scattering from 1 ML and one part scattering from 2 ML.

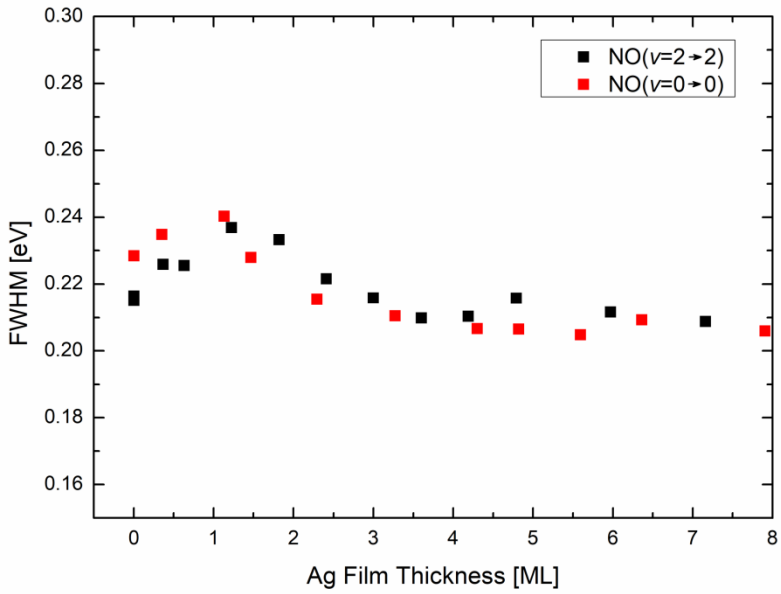

S4: FWHM of the kinetic energy distributions for NO($v = 2 \rightarrow 2$) and NO($v = 0 \rightarrow 0$) derived from the obtained fits. In a first approximation, we observe a constant value; there might be a slight increase between 0-2 ML Ag/Au indicating that the resulting distributions are a mix of the two components which are scattering from different areas of completed monolayers.

This idea is tested by performing NO($v = 2 \rightarrow 2$) scattering from a wedge sample of 0 to 2.4 ML Ag/Au(111). Arrival time distributions were recorded for several film thicknesses between 0 and 1 ML as shown in Fig. S5. We apply the model $(1 - x)A(t) + xB(t)$ describing a superposition of the fit functions obtained from pure Au(111) ($A(t)$) and 1 ML Ag/Au(111) ($B(t)$) with x as the mixing parameter. The model reproduces scattering curves of fractional monolayers with reasonable agreement. To conclude, although the change of the peak timing is small in this thickness region, our data suggests that intermediate Ag thicknesses can be described by curves obtained from completed layers.

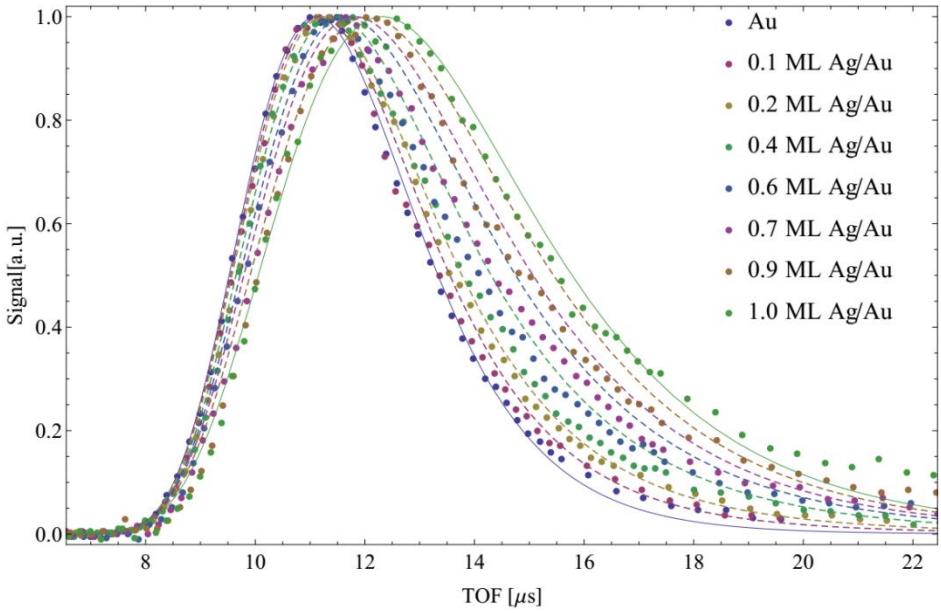

S5: Arrival time distributions of NO($v = 2 \rightarrow 2$) between 0 and 1 ML Ag/Au (dotted). The points for Au(111) and 1 ML Ag/Au(111) were fitted in the usual manner resulting in fit functions $A(t)$ and $B(t)$ (solid lines). Now, the superposition model (see body text) was applied for thicknesses between 0 and 1 ML (dashed line) obtaining reasonable agreement with the data.

Analogously to Fig. 3, CO($v = 2 \rightarrow 2$) TOF distributions and kinetic energy distributions are depicted in Fig. S6 and Fig. S7.

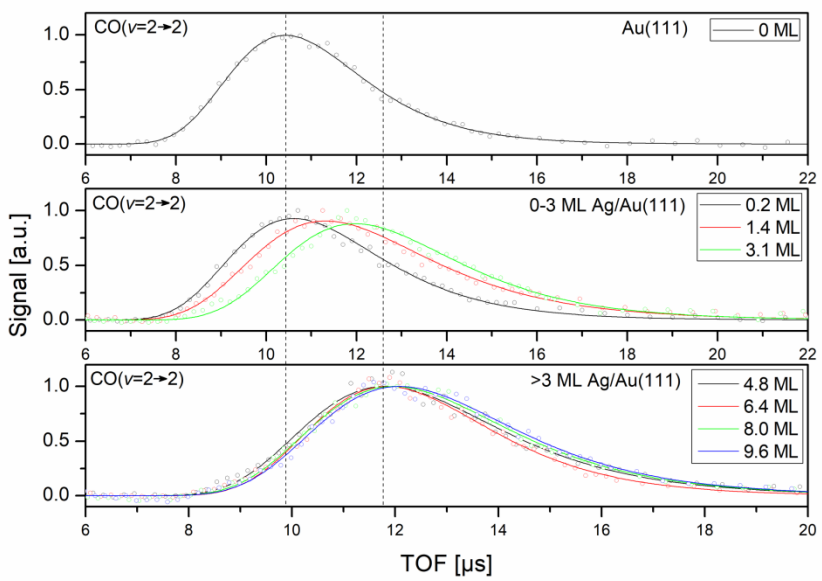

Fig. S6: Arrival time distributions of CO($v = 2 \rightarrow 2$) scattering from a 0-9.6 ML wedge of Ag/Au(111). Peak timings of both limiting cases (clean Au and bulk limit of Ag/Au) are marked by two dashed vertical lines.

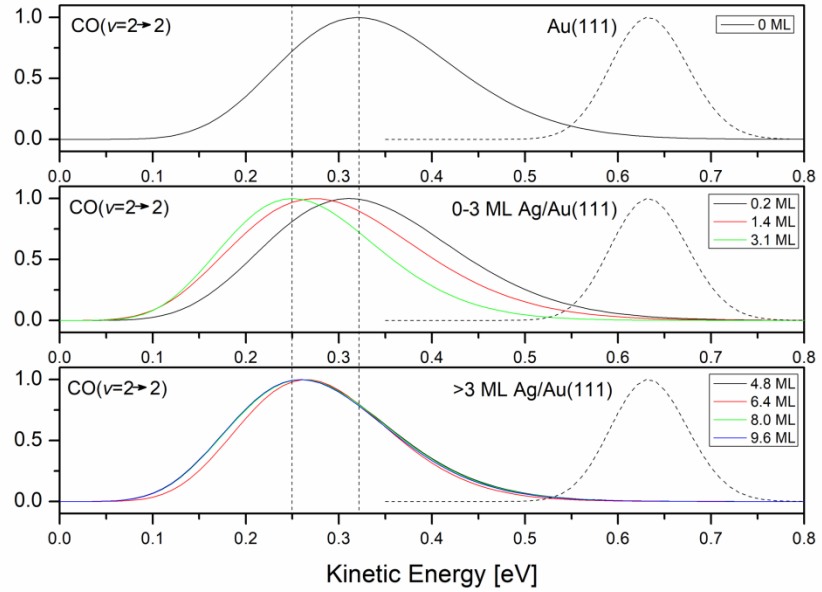

Fig. S7: Kinetic energy distributions of CO($v = 2 \rightarrow 2$) as determined from the fits depicted in Fig. S6.

2. NO($v = 0 \rightarrow 0$) scattering from bulk Au(111) and Ag(111)

This section contains additional information about the data set for NO($v = 0 \rightarrow 0$) scattering that is plotted in Figure 5 of the main manuscript.

In a prior study of NO scattering from bulk crystal surfaces, several gas mixtures with different incident energies were prepared and scattered off bulk surfaces of Au(111) and Ag(111). A characterization of those gas mixtures is shown in Table S1. The incident velocity distribution is represented by a function of the form $P(v) = Av^3 \exp\left(\frac{(v-v_0)^2}{\alpha^2}\right)$, from which the mean velocity $\langle v \rangle = \frac{\int_0^\infty vP(v)dv}{\int_0^\infty P(v)dv}$ can be obtained.

Table S1: Characterization of the gas mixtures used for scattering from bulk Au(111) and Ag(111).

Gas mixture	$\langle E_i \rangle$ [eV]	FWHM [eV]	$\langle v \rangle$[m·s^{-1}]	α[m·s^{-1}]
20% NO/ 30% Kr/ 50% Ne	0.07	0.01	669	27
15% NO/ 85% Ne	0.12	0.02	863	38
7% NO/ 40% Ne/ 53% H_2	0.21	0.04	1163	39
20% NO/ 80% H_2	0.36	0.07	1514	87
15% NO/ 85% H_2	0.4	0.05	1599	62
10% NO/ 90% H_2	0.49	0.07	1776	80
6% NO/ 94% H_2	0.73	0.11	2170	100
2% NO/ 98% H_2	0.92	0.15	2426	120

The data for NO($v = 0 \rightarrow 0$) scattering from Au(111) and Ag(111) was measured with the same machine used for NO($v = 0 \rightarrow 0$) scattering from thin films. Similarly, as depicted in Fig. 2a, molecules were vibrationally "tagged" by IR excitation into a higher vibrational state after scattering from the surface and were detected in a state-selective manner by UV ionization using REMPI. However, the flight length between the IR and the UV spot was slightly longer (20.3 mm (bulk crystal study) vs 14.9 mm (thin film study). TOF spectra were acquired for a number of different rotational states between $J = 4.5$ and $J = 36.5$ by setting the IR and the UV laser to the corresponding wavelengths. Representative examples of TOF spectra are depicted in Fig. S8.

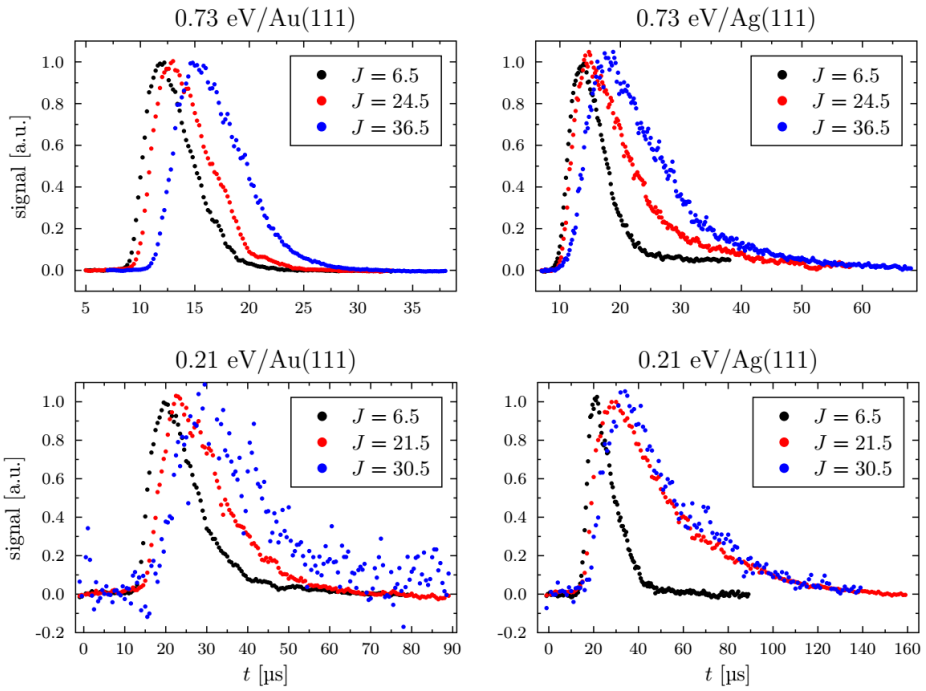

Fig. S8: Comparison of TOF spectra of NO(v = 0 ⟶ 0) scattering from bulk Au(111) and Ag(111)for $\langle E_i \rangle$ = 0.73 eV (top row) and $\langle E_i \rangle$ = 0.21 eV (bottom row) at rotational energies of 0.01 eV (J = 6.5), 0.13 eV (J = 24.5)and 0.29 eV (J = 36.5).

A plot of the mean translation energy vs rotational energy is depicted in Fig. S9.

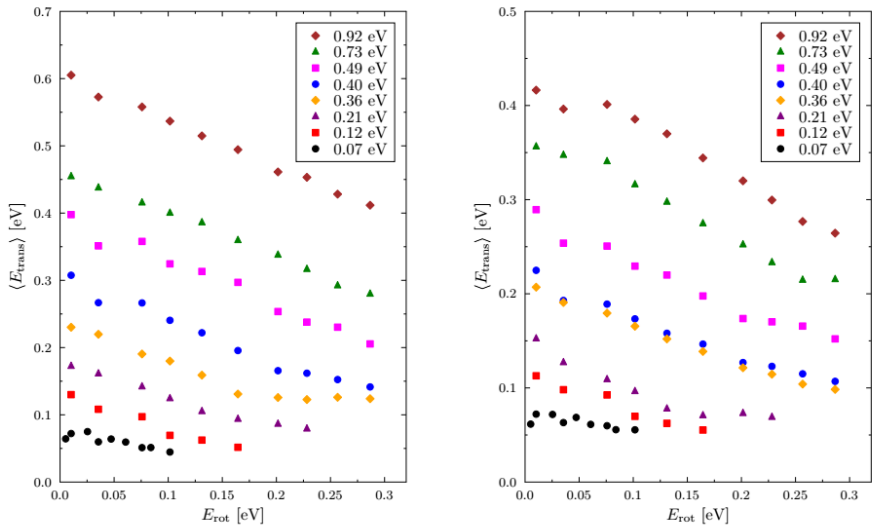

Fig. S9: T-R plots for NO(v = 0 ⟶ 0)scattering from bulk Au(111) and Ag(111) at various incidence energies (0.07 to 0.92 eV) combined for each surface.

The mean translational energy for a gas mixture at a defined surface was obtained from the limit of a rotationally-elastic collision$\lim_{E_{\mathrm{rot}}\to 0}\langle E_{\mathrm{trans}}\rangle$ by extrapolating the observed data.

The NO($v = 0 \rightarrow 0$) scattering data obtained in that bulk crystal study showed a systematic difference towards all other studies measured at the same machine. Compared to the NO($v = 0 \rightarrow 0$) data from the thin film study or an investigation about NO($v = 3 \rightarrow 3$) scattering from Au(111) (Golibrzuch et al., *Phys. Chem. Chem. Phys.* **2014**, *16*, 7602-10), the experimentally measured final translational energy distributions appeared to be scaled by a constant factor of 1.25, resulting in seemingly broader distributions with higher mean translational energy. We assign this effect to the longer flight length used in the bulk crystal study on NO($v = 0 \rightarrow 0$) scattering. Assuming the same size of the ionization spot, a longer flight length leads to a higher dispersion of molecules. To allow a direct comparison with the thin film study data, the displayed data points for NO($v = 0 \rightarrow 0$) from Au(111) and Ag(111) (Fig. 5) were corrected by dividing by the mentioned factor.

3. Theoretical Calculations

3.1 Potential Well

The DFT calculations were performed using VASP (vers. 5.3.5).[1-4] The electron-core interactions were described by projected-augmented-wave (PAW) potentials and the Kohn-Sham eigenstates by plane-waves with a cut-off energy of 400 eV. For exchange-correlation, the RPBE functional on the GGA-level was employed. Furthermore, the Scheffler-Tkatchenko method was used to correct for van-der-Waals interactions.[5]

The surface was modeled by a $p(3 \times 3)$ cell with 4 layers with an optimized lattice constant of 4.20 Å. This is slightly different to the experimental value of 4.08 Å. The layers consist of pure Au and were successively replaced by Ag from the uppermost layer to the bottom layer. Since VASP employs periodic boundary conditions, the simulation cell is repeated in the directions of the 3 lattice vectors. To avoid interactions between repeated images of the system in z-direction a vacuum distance of 20 Å was used. The reciprocal space was sampled with a $4 \times 4 \times 1$ k-point grid.

The interaction potential between surface and molecule was calculated by varying the molecule's center-of-mass distance Z_{CM} to the uppermost layer of the surface. The molecule was oriented with the C atom towards the surface above a top site of the surface. The bond distance of the molecule was fixed according to an excited vibrational state of $v = 2$.

The calculations show that deposition of Ag atoms has only negligible effect on the binding well (Fig. S10). The biggest difference in interaction potential is found after deposition of 1 ML which does not offer an explanation for the 0-3 ML transition of the mean final translational energies.

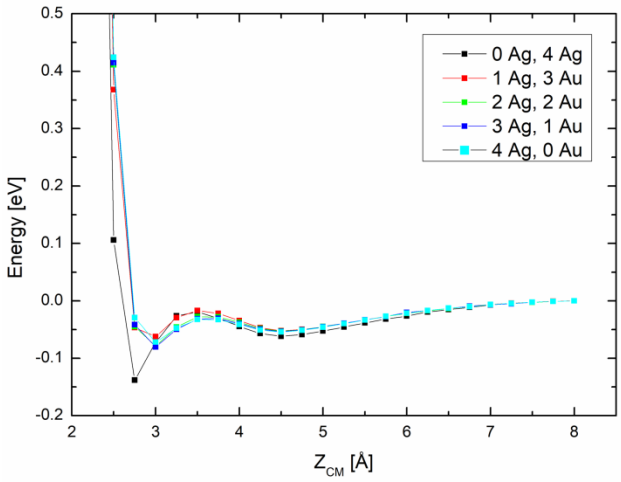

S10: Thickness-dependent potential of CO(v = 2) scattering on Ag/Au. The deposition of Ag onto the surface leads to a negligible change (<0.1 eV) after the first monolayer. As a consequence, the change of the potential well cannot explain the trend observed for the translational inelasticity.

3.2 Phonon Frequencies

To generate the phonon spectra, the Phonopy[6] software package was used. This package calculates the force constants within the finite displacement method. Hence, every atom in the system is displaced two times by a distance about 0.1 Å and then the energy for all generated configurations is calculated (via VASP). The output from these calculations is used by Phonopy to calculate the force constants between all atoms. With these constants and information about the employed simulation cell, Phonopy can construct the phonon spectrum.

As initial input configuration for the calculation of the phonon spectra, we modeled a $p(1 \times 1)$ cell with 4 layers and 20 Å vacuum between images in z-direction. Please note that rather complex phonon spectra arise due to the employment of periodic boundary conditions. To account for the smaller cell, a denser k-point grid of $12 \times 12 \times 1$ was used. Here, the interaction between the electrons was described by the RPBE functional. The cell was geometry optimized until the force on every atom was < 0.01 eV/Å and then used as input for Phonopy to generate the displaced configurations.

The phonon spectra in Fig. S11 were obtained by using the procedure describe above and replacing Au atoms/layers by Ag from top to bottom of the slab, respectively. The highest

frequency as the cutoff-frequency was extracted and is plotted against the film thickness in Fig. 5 of the main manuscript. We interpret this frequency as the Debye frequency.

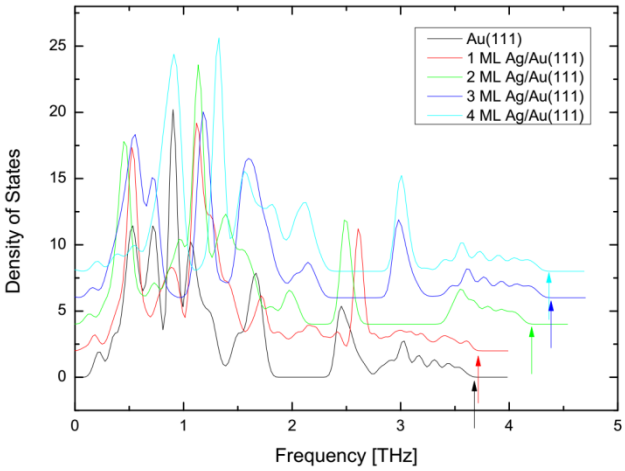

Fig. S11: Thickness-dependent phonon spectra of Ag/Au. The highest frequency (Debye frequency) is marked by a small arrow.

It was confirmed that the $1 \times 1 \times 4$ slab does not introduce artifacts due to the choice of a small model of only four layers. Phonon spectra for 4 ML Ag/Au were calculated for slabs of the size $1 \times 1 \times z$ with $z = 4, 7, 11$ denoting the number of the layers, upper 4 of which consist of Ag atoms and the rest of Au atoms. The number of the layers z affects the phonon spectra obtained, but the highest frequency remains almost the same (see Fig. S12).

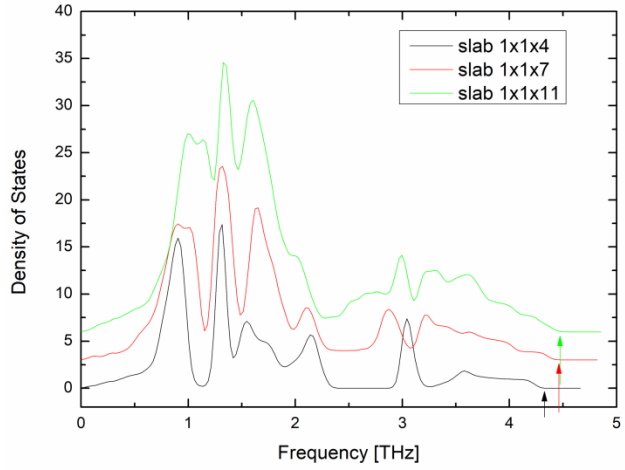

S12: Phonon spectra for the film of 4 ML Ag/Au calculated for $1 \times 1 \times z$ slabs of $1 \times 1 \times 4, 7, 11$.

References

1. Kresse, G.; Furthmüller, J., Efficient Iterative Schemes for Ab Initio Total-Energy Calculations Using a Plane-Wave Basis Set. *Phys. Rev. B* **1996**, *54*, 11169.
2. Kresse, G.; Furthmüller, J., Efficiency of Ab-Initio Total Energy Calculations for Metals and Semiconductors Using a Plane-Wave Basis Set. *Comput. Mater. Sci.* **1996**, *6*, 15-50.
3. Kresse, G.; Hafner, J., Ab Initio Molecular Dynamics for Liquid Metals. *Phys. Rev. B* **1993**, *47*, 558.
4. Kresse, G.; Hafner, J., Ab Initio Molecular-Dynamics Simulation of the Liquid-Metal–Amorphous-Semiconductor Transition in Germanium. *Phys. Rev. B* **1994**, *49*, 14251.
5. Tkatchenko, A.; Scheffler, M., Accurate Molecular Van Der Waals Interactions from Ground-State Electron Density and Free-Atom Reference Data. *Phys. Rev. Lett.* **2009**, *102*, 073005.
6. Togo, A.; Tanaka, I., First Principles Phonon Calculations in Materials Science. *Scr. Mater.* **2015**, *108*, 1.